Electron-pair analysis for doubly excited ridge states. II. $L=1$

Lijun Zhang* and A. R. P. Rau
Department of Physics and Astronomy, Louisiana State University, Baton Rouge, Louisiana 70803-4001
(Received 11 June 1993)

We study doubly excited ridge states using hyperspherical coordinates. Viewing the two electrons as a pair, as we did for ^1S states in a previous paper [Phys. Rev. A **46**, 6933 (1992)], here we extend to the $L=1$ states. By diagonalizing the potential energy within manifolds of fixed grand angular momentum, we get simple, even analytical, expressions for the effective charge. Upper bounds for the energies of the $L=1$ states are derived through the Runge-Kutta numerical procedure.

PACS number(s): 31.50.+w, 31.10.+z

I. INTRODUCTION

This paper reports the results for doubly excited $^1P^o$, $^3P^o$, $^1P^e$, and $^3P^e$ resonant states in H^- and He. This work is an extension of our previous work [1] in which we only considered ^1S states and had also neglected major radial-derivative coupling terms.

Experimental and theoretical work has shown that doubly excited states fall broadly into two classes [2,3], distinguished by the nature of their excitations. The two electrons may have either comparable or disparate excitation. Correspondingly, the states have been named as "ridge" and "valley," respectively. Our previous paper has dealt with symmetrical ridge states of $L=0$. In such states the two electrons are equivalent in their excitation relative to the residual "grandparental ion" [4]. In this paper we deal with similar $L=1$ states. As before, we continue to use hyperspherical coordinates which are defined as $R=(r_1^2+r_2^2)^{1/2}$ and $\alpha=\tan^{-1}(r_2/r_1)$. In this coordinate system, R measures the size and $\Omega=(\alpha,\theta_1,\phi_1,\theta_2,\phi_2)$ denotes the orientation of the electrons in the six-dimensional configuration space of the system. In these coordinates, the system's potential can be written as

$$V(\mathbf{r}_1,\mathbf{r}_2)=\frac{C(\alpha,\theta_{12})}{R}=\frac{1}{R}\left[-\frac{Z}{\cos\alpha}-\frac{Z}{\sin\alpha}+\frac{1}{[1-\sin(2\alpha)\cos\theta_{12}]^{1/2}}\right], \tag{1}$$

where $\theta_{12}=\cos^{-1}(\mathbf{r}_1\cdot\mathbf{r}_2)$ and $\cos\theta_{12}=\cos\theta_1\cos\theta_2+\sin\theta_1\sin\theta_2\cos(\phi_1-\phi_2)$. The potential energy C/R depends explicitly on θ_{12}. It then seems natural to choose θ_{12} as one angular coordinate as we did before for ^1S. However, we prefer to use $(\theta_1,\phi_1,\theta_2,\phi_2)$ as angular coordinates because of other advantages when $L\neq 0$. In Sec. II we will give details of the calculations and discuss the results briefly in Sec. III.

II. CALCULATIONAL PROCEDURE

The two-electron Schrödinger equation in hyperspherical coordinates is

$$\left[\frac{1}{2}\left[-\frac{d^2}{dR^2}+\frac{\Lambda^2+\frac{15}{4}}{R^2}\right]+\frac{C(\alpha,\theta_{12})}{R}\right](R^{5/2}\Psi(R,\Omega))=ER^{5/2}\Psi(R,\Omega)\ . \tag{2a}$$

The squared grand angular momentum operator Λ^2 in these variables is given by

$$\Lambda^2=-[\sin\alpha\cos\alpha]^{-2}\frac{d}{d\alpha}\left[\sin^2\alpha\cos^2\alpha\frac{d}{d\alpha}\right]+\frac{l_1^2}{\cos^2\alpha}+\frac{l_2^2}{\sin^2\alpha}\ , \tag{2b}$$

where l_1^2 and l_2^2 are the squared orbital angular momentum operators [2] for the two electrons.

The eigenvalues and eigenstates of Λ^2 are

$$\Lambda^2\Phi^{S\pi}_{n_{RC}l_1l_2LM}(\Omega)=\lambda(\lambda+4)\Phi^{S\pi}_{n_{RC}l_1l_2LM}(\Omega)\ , \tag{3a}$$

$$\lambda=l_1+l_2+2n_{RC}=0,1,2,\ldots, \tag{3b}$$

$$\Phi^{S\pi}_{n_{RC}l_1l_2LM}(\Omega)=c[\phi_{n_{RC}l_1l_2LM}(\Omega)+(-)^{l_1+l_2-L+S+n_{RC}}\times\phi_{n_{RC}l_2l_1LM}(\Omega)]\ , \tag{3c}$$

$$c=\begin{cases}\frac{1}{\sqrt{2}} & \text{if } l_1\neq l_2\\ \frac{1}{2} & \text{if } l_1=l_2\ ,\end{cases} \tag{3d}$$

$$\phi_{n_{RC}l_1l_2LM}(\Omega)=N_{n_{RC}l_1l_2}(\cos^{l_1}\alpha)(\sin^{l_2}\alpha)\times Y_{l_1l_2LM}(\hat{\mathbf{r}}_1,\hat{\mathbf{r}}_2)\times{}_2F_1(-n_{RC},n_{RC}+l_1+l_2+2,l_2+\tfrac{3}{2};\sin^2\alpha)\ , \tag{3e}$$

$$Y_{l_1l_2LM}(\hat{\mathbf{r}}_1,\hat{\mathbf{r}}_2)=\sum_{m_1,m_2}(l_1l_2LM|l_1m_1,l_2m_2)\times Y_{l_1m_1}(\hat{\mathbf{r}}_1)Y_{l_2m_2}(\hat{\mathbf{r}}_2)\ , \tag{3f}$$

and

$$N_{n_{RC}l_1l_2}=2^{l_1+l_2+1}\frac{l_2!}{(2l_2+1)!}\left[\frac{(2n_{RC}+2l_2+1)!(n_{RC}+l_1)!}{(n_{RC}+l_2)!(2n_{RC}+2l_1+1)!}\right]^{1/2}\times\left[\frac{2(l_1+l_2+2n_{RC}+2)(n_{RC}+l_1+l_2+1)!}{n_{RC}!\pi}\right]^{1/2}. \tag{3g}$$

Here Y is the familiar coupled spherical harmonic which includes a Clebsch-Gordan coefficient, ${}_2F_1$ is a hypergeometric function which, for the integer values of the radial correlation quantum number n_{RC} of interest, is proportional to a Jacobi polynomial, and $N_{n_{RC}l_1l_2}$ is a normalization constant.

In the previous paper we restricted ourselves to the $L=0$ case where the above equations simplify dramatically. When $L=1$, we have two cases: if $l_1\neq l_2$ with $|l_1-l_2|=1$, then λ $(=l_1+l_2+2n_{RC})$ and parity are odd, whereas if $l_1=l_2$, λ $(=l_1+l_2+2n_{RC})$ and parity are even. In the next three subsections, we will discuss even- and odd-parity states separately.

A. P^o states

In P^o states, the two individual angular momenta l_1 and l_2 are not equal and $Y_{l_1l_210}$ does not simplify as in the $L=0$ case. The wave function in this case is

$$\Phi_{n_{RC}l_1l_2}(\Omega)=\frac{1}{\sqrt{2}}[\phi_{n_{RC}l_1l_210}(\Omega)+(-)^{n_{RC}+S}\phi_{n_{RC}l_2l_110}(\Omega)], \tag{4}$$

with $S=0$ for singlet states and $S=1$ for triplet states. The matrix elements in each λ subspace are

$$\langle\Phi_{n_{RC}l_1l_2}|C(\alpha,\theta_{12})|\Phi_{n'_{RC}l'_1l'_2}\rangle . \tag{5}$$

It is useful to divide the charge operator into

$$C(\alpha,\theta_{12})=U(\alpha)+W(\alpha,\theta_{12}), \tag{6}$$

with

$$U(\alpha)=-\frac{Z}{\cos\alpha}-\frac{Z}{\sin\alpha}, \tag{7}$$

$$W(\alpha,\theta_{12})=[1-\sin(2\alpha)\cos\theta_{12}]^{-1/2}. \tag{8}$$

Then

$$\langle\Phi_{n_{RC}l_1l_2}|C(\alpha,\theta_{12})|\Phi_{n'_{RC}l'_1l'_2}\rangle = \int\int d\Omega\, C(\alpha,\theta_{12})\Phi_{n_{RC}l_1l_2}\Phi_{n'_{RC}l'_1l'_2} = \int_0^{\pi/2}d\alpha\frac{\sin^2 2\alpha}{4}U(\alpha)\Phi_{n_{RC}l_1l_2}\Phi_{n'_{RC}l'_1l'_2}\delta_{l'_1l_1}\delta_{l'_2l_2} + \int\int d\Omega\, W(\alpha,\theta_{12})\Phi_{n_{RC}l_1l_2}\Phi_{n'_{RC}l'_1l'_2}. \tag{9}$$

We have dropped the indices S, π, L, and M because these values are already fixed.

Only the second term in (9) involves the coupling of different spherical harmonics. We briefly outline how to calculate this coupling. Expanding $W(\alpha,\theta_{12})$ in the form

$$[1-\sin(2\alpha)\cos\theta_{12}]^{-1/2}=\begin{cases}\displaystyle\sum_{k=0}^{\infty}\frac{\tan^k\alpha}{\cos\alpha}P_k(\cos\theta_{12}), & 0\le\alpha\le\frac{\pi}{4}\\ \displaystyle\sum_{k=0}^{\infty}\frac{\cot^k\alpha}{\sin\alpha}P_k(\cos\theta_{12}), & \frac{\pi}{4}\le\alpha\le\frac{\pi}{2},\end{cases} \tag{10}$$

define $A[k,l_1,l_2,l'_1,l'_2]$ as

$$A[k,l_1,l_2,l'_1,l'_2]=\langle Y_{l_1l_210}|P_k(\cos\theta_{12})Y_{l'_1l'_210}\rangle =(-)^{l'_1+l_2+L}\langle l_1\|C^k\|l'_1\rangle\langle l_2\|C^k\|l'_2\rangle\times\begin{Bmatrix}l_1 & l_2 & L\\ l'_2 & l'_1 & k\end{Bmatrix}, \tag{11}$$

where

$$\langle l_i\|C^k\|l_j\rangle=(-)^{l_i}\sqrt{(2l_i+1)(2l_j+1)}\times\begin{bmatrix}l_i & k & l_j\\ 0 & 0 & 0\end{bmatrix}, \tag{12}$$

$\begin{pmatrix}l_i & k & l_j\\ 0 & 0 & 0\end{pmatrix}$ being a 3-j symbol and $\begin{Bmatrix}l_1 & l_2 & L\\ l'_2 & l'_1 & k\end{Bmatrix}$ a 6-j symbol. Then, with standard expressions for these symbols [5], we get

$$A[k,l_1,l_2,l'_1,l'_2]=(-)^{l'_1+1+g_1+g_2+l_1}\sqrt{(2l_1+1)(2l_2+1)(2l'_1+1)(2l'_2+1)}\times\left[\frac{(2g_1-2l_1)!(2g_1-2k)!(2g_1-2l'_1)!}{(2g_1+1)!}\right]^{1/2}\frac{g_1!}{(g_1-l_1)!(g_1-k)!(g_1-l'_1)!}\times\left[\frac{(2g_2-2l_2)!(2g_2-2k)!(2g_2-2l'_2)!}{(2g_2+1)!}\right]^{1/2}\frac{g_2!}{(g_2-l_2)!(g_2-k)!(g_2-l'_2)!}B(X), \tag{13}$$

TABLE I. Eigenvalues of effective charge operator $C_{\lambda Q}$ for $^1P^o$ states of He with $\lambda \leq 11$.

λ \ Q	0	1	2	3	4	5
1	−5.350 11					
3	−4.624 53	−6.924 50				
5	−4.339 24	−5.806 63	−7.559 65			
7	−4.169 30	−5.345 84	−6.266 37	−8.311 88		
9	−4.050 00	−5.079 98	−5.710 90	−6.871 70	−8.707 76	
11	−3.957 92	−4.901 39	−5.386 90	−6.224 12	−7.192 48	−9.210 80

where $g_1=(l_1+l_1'+k)/2$ and $g_2=(l_2+l_2'+k)/2$. The last term in (13) is given by

$$B(X)=(-)^X\left[\frac{X(X+1)(X-2k-1)(X-2k)}{(2l_1-1)2l_1(2l_1+1)(2l_1'-1)2l_1'(2l_1'+1)}\right]^{1/2}, \tag{14}$$

if $X=k+l_1+l_1',l_2=l_1-1$, and $l_2'=l_1'-1$, and the same expression with subscripts 1 replaced by 2 if $X=k+l_1+l_1'+2$, $l_2=l_1+1$, $l_2'=l_1'+1$, whereas

$$B(X)=(-)^X\left[\frac{(X-2l_1')(X-2l_1'-1)(X-2l_1+1)(X-2l_1+2)}{(2l_1'+1)(2l_1'+2)(2l_1'+3)(2l_1-1)2l_1(2l_1+1)}\right]^{1/2}, \tag{15}$$

if $X=k+l_1+l_1'$, $l_2=l_1-1$ and $l_2'=l_1'+1$, with primed and unprimed entries interchanged when $X=l_1+l_1'+k$, $l_2=l_1+1$, and $l_2'=l_1'-1$.

Inserting the coupling coefficient A into (9), and evaluating the α integral numerically, we can diagonalize the matrix in (5). Results are given in Table I and the eigenvalues plotted vs the quantum number Q in Fig. 1 for $\lambda \leq 27$. The eigenvalues are labeled by $Q=0,1,\ldots,$ the maximum value of Q is $\frac{1}{2}(\lambda-1)$.

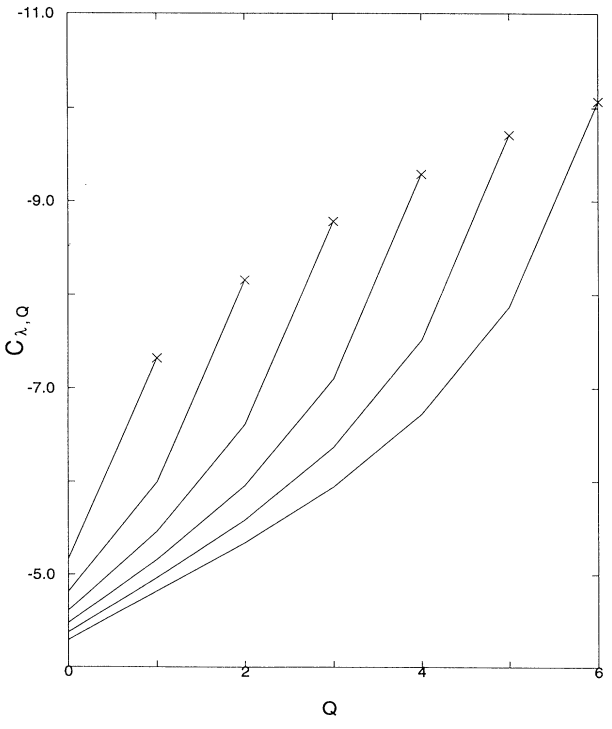

FIG. 1. Effective charge for $^1P^o$ states. Results of numerical diagonalization of (9) are shown as continuous curves. Crosses give maximum eigenvalue as given by the approximate analytical expression in (17).

B. Eigenvalues for $^1P^o$ states

As in the previous paper, we again find that the extreme eigenvalues are well approximated by the diagonal matrix elements with the lowest and highest n_{RC} values. In either of these cases, Φ in (4) takes a simple form and the matrix element can be evaluated analytically. We are interested in only the lowest eigenvalue for each λ to get the most attractive potential. This has $l_1=1$ and $l_2=0$ and the highest value of $n_{RC}=(\lambda-1)/2$. When n_{RC} is even, the corresponding states are called n_+, and when n_{RC} is odd, the corresponding states are called n_-. The wave function, therefore, reduces to

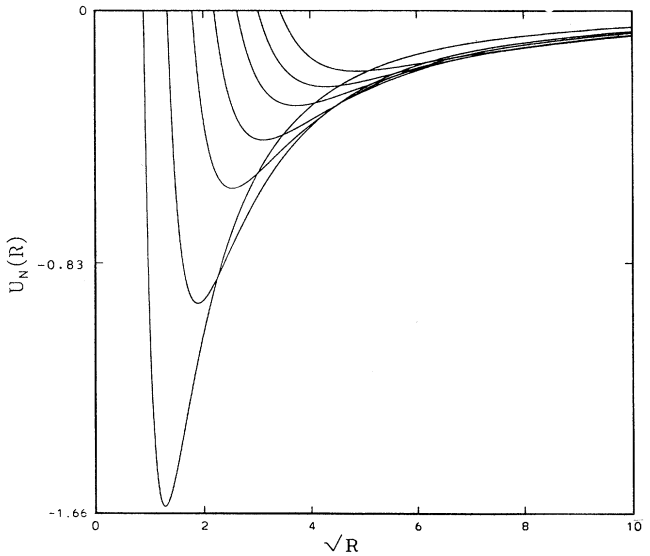

FIG. 2. Potential wells $U(R)=(\lambda+3/2)(\lambda+5/2)/2R^2+C_{\lambda Q=(\lambda-1)/2}/R$, with $\lambda=1$, 3, 5, 7, 9, 11, and 13 and $Z=2$ for $^1P^o$.

TABLE II. Eigenvalues of effective charge operator $C_{\lambda Q}$ for $^1P^e$ states of He with $\lambda \leq 24$.

λ \ Q	0	1	2	3	4	5
4	−6.084 98					
8	−5.170 68	−7.325 64				
12	−4.818 08	−5.997 67	−8.158 96			
16	−4.615 89	−5.467 40	−6.618 24	−8.158 96		
20	−4.477 98	−5.168 78	−5.963 46	−7.104 98	−9.291 45	
24	−4.374 41	−4.971 64	−5.591 52	−6.373 59	−7.517 86	−9.712 56

$$\Phi_{\lambda n_{RC}}(\Omega)=N_{\lambda n_{RC}}\left\{\frac{1}{\cos\alpha\sin(2\alpha)}\{(n_{RC}+2)\sin[2(n_{RC}+1)\alpha]+(n_{RC}+1)\sin[2(n_{RC}+2)\alpha]\}Y_{1010}(\hat{\mathbf{r}}_1,\hat{\mathbf{r}}_2)+(-)^{n_{RC}+S}\frac{1}{\sin\alpha\sin(2\alpha)}\{(n_{RC}+2)\sin[2(n_{RC}+1)\alpha]-(n_{RC}+1)\sin[2(n_{RC}+2)\alpha]\}Y_{0110}(\hat{\mathbf{r}}_1,\hat{\mathbf{r}}_2)\right\}, \quad (16)$$

where $N_{\lambda n_{RC}}=2/[(n_{RC}+1)(n_{RC}+2)\pi]^{1/2}$ is the normalization constant.

The evaluation of matrix elements of C

$$C_{\lambda,Q=(\lambda-1)/2}=\langle\Phi_{\lambda n_{RC}}(\Omega)|C(\alpha,\theta_{12})|\Phi_{\lambda n_{RC}}(\Omega)\rangle, \quad (17)$$

analytically requires some algebra, details of which are given in [6]. For large λ this expression for the effective charge simplifies further:

$$C_{\lambda Q=(\lambda-1)/2}\simeq-\frac{4}{\pi}\{Z[\gamma-\tfrac{1}{2}+\ln(4\lambda+10)]-1\}, \quad (18)$$

where $\gamma=0.577\,21$ is Euler's constant. With this effective charge, we have potential wells for each of the λ values as displayed in Fig. 2.

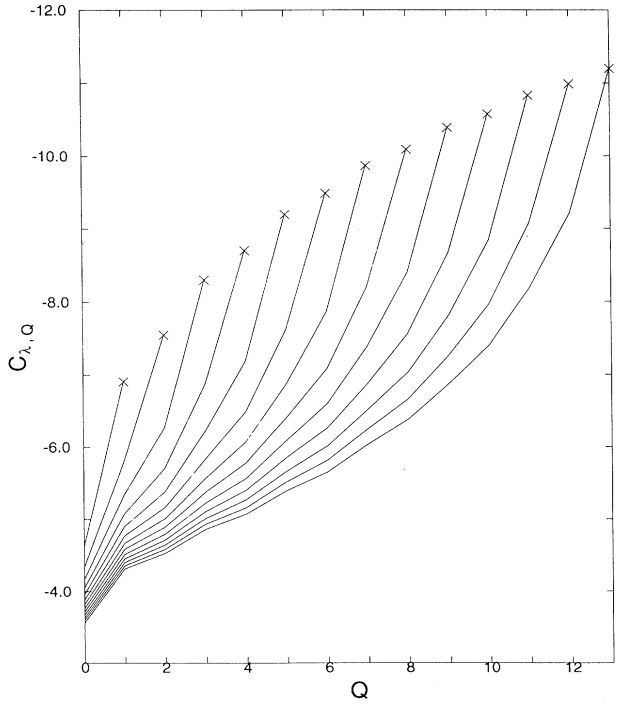

FIG. 3. Effective charge for $^1P^e$ states. Results of numerical diagonalization of (9) are shown as continuous curves. Crosses give maximum eigenvalue as given by the approximate analytical expression in (22).

C. P^e states

In P^e states, the two individual angular momenta l_1 and l_2 are equal. The wave function in this case is (for $M=0$)

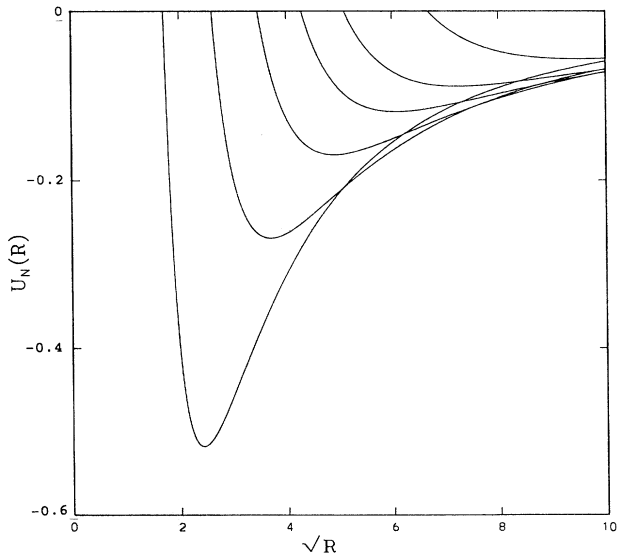

FIG. 4. Potential wells $U(R)=(\lambda+3/2)(\lambda+5/2)/2R^2+C_{\lambda Q=(\lambda-4)/4}/R$, with $\lambda=4$, 8, 12, 16, 20, 24, and 28 and $Z=2$ for $^1P^e$.

$$\Phi^{S\pi}_{n_{RC}l_1l_2LM}(\Omega)=\Phi^{S\pi}_{n_{RC}ll10}(\Omega)$$
$$=\tfrac{1}{2}[1+(-1)^{S+1+n_{RC}}]\phi_{n_{RC}ll}(\Omega)\ . \qquad (19)$$

For singlet states, n_{RC} is odd, and for triplet states, it is even. Upon diagonalizing the effective charge operator $C(\alpha,\theta_{12})$ in a λ subspace, eigenvalues for $^1P^e$ states are as shown in Table II. The plot of the eigenvalues vs the quantum number Q as a continuous curve is given in Fig. 3. The maximum Q value is $\frac{1}{4}(\lambda-4)$. The most attractive eigenvalue that we are interested in has the highest n_{RC}. In $^1P^e$ states, this means $n_{RC}=(\lambda-2)/2$, $l_1=l_2=1$. The wave function has a simple form

$$\Phi_{\lambda n_{RC}}(\Omega)=N_{\lambda n_{RC}}\frac{1}{\sin^2(2\alpha)}\{(n_{RC}+3)\sin[2(n_{RC}+1)\alpha]$$
$$-(n_{RC}+1)\sin[2(n_{RC}+3)\alpha]\}$$
$$\times Y_{1110}(\hat{\mathbf{r}}_1,\hat{\mathbf{r}}_2)\ , \qquad (20)$$

where

$$N_{\lambda n_{RC}}=2/[(n_{RC}+1)(n_{RC}+3)\pi]^{1/2}\ . \qquad (21)$$

The effective charge

$$C_{\lambda,Q=(\lambda-4)/4}=\langle\Phi_{\lambda n_{RC}}(\Omega)|C(\alpha,\theta_{12})|\Phi_{\lambda n_{RC}}(\Omega)\rangle \qquad (22)$$

can again be evaluated and an approximate analytical expression derived [6]. This effective charge can be simplified further as

$$C_{\lambda Q=(\lambda-4)/4}\simeq=-\frac{4}{\pi}\{Z[\gamma-2+\ln(4\lambda+10)]$$
$$+(Z-1)+0.15\}\ . \qquad (23)$$

Using these effective charges, we get the potential wells for each λ as shown in Fig. 4.

D. Coupled potential wells

In order to get more accurate results, we need to consider the coupling between different λ. As observed before, in each λ subspace only the lowest potential wells seem to play a dominant role. Therefore, we will only keep the lowest eigenvalue for each λ. However, we now also calculate the off-diagonal matrix elements between different λ:

$$C_{\lambda\lambda'}=\langle\Phi_{\lambda n_{RC}}(\Omega)|C(\alpha,\theta_{12})|\Phi_{\lambda' n'_{RC}}(\Omega)\rangle\ . \qquad (24)$$

For any $\lambda_{\max}$, we can diagonalize the matrix given by (17) and (24) by retaining λ values from 1 to $\lambda_{\max}$ for $^1P^o$ states and from 4 to $\lambda_{\max}$ for $^1P^e$ states at each R value. From the corresponding eigenvalues at each R, we construct the potential wells $U_N(R)$ as shown in Fig. 5 for $^1P^o$ and Fig. 6 for $^1P^e$ states. If we choose $\lambda_{\max}=121$ we need to diagonalize numerically 61×61 matrix elements in the $^1P^o$ case and 30×30 in the $^1P^e$ case.

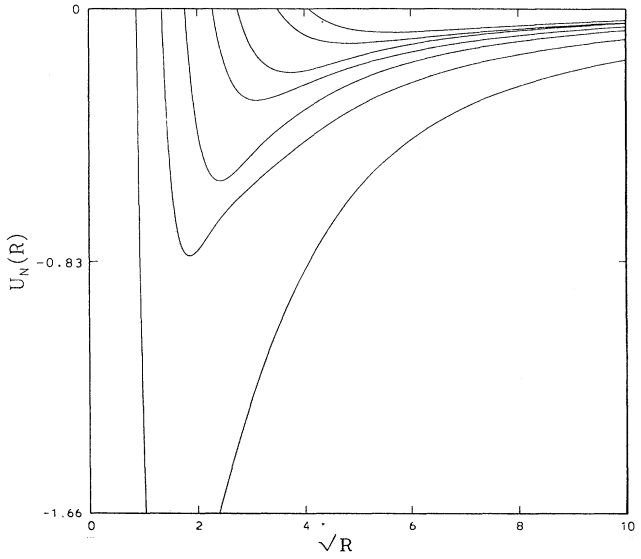

FIG. 5. Potential curves for $^1P^o$ by diagonalizing the matrix given by (17) and (24) with $\lambda=1$, 3, 5, 7, 9, 11, and 13 and $Z=2$.

To solve for the eigenvalues of doubly excited states, the eigenvectors obtained above at each R provide a basis $\psi_N(R;\Omega)$ for expansion of the full wave function in (2a):

$$\Psi(R,\Omega)=\sum_N F_N(R)\psi_N(R;\Omega)\ . \qquad (25)$$

Inserting this into the Schrödinger equation (2a) leads to coupled differential equations for $\mathbf{F}(R)$, or equivalently for $\mathbf{G}(R)=R^{5/2}\mathbf{F}(R)$. Multiplying by $\psi_N(R;\Omega)$ and in-

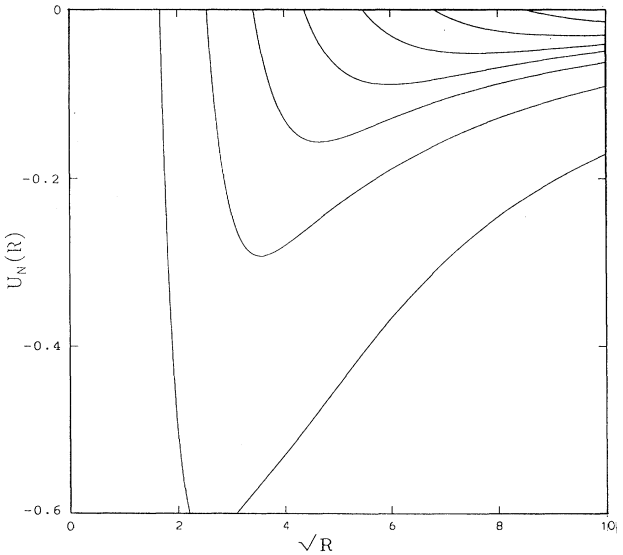

FIG. 6. Potential curves for $^1P^e$ by diagonalizing the matrix given by (22) and (24) with $\lambda=4$, 8, 12, 16, 20, 24, and 28 and $Z=2$.

TABLE III. Eigenvalues (in a.u.) calculated by Eq. (30) for H^- $^1P^o$ states, where $\lambda_{max}=121$.

	Eigenvalue					
$_n(K,T)^A_N$	Present	Other [Ref.]	Ref. [15]	Ref. [16]	Ref. [12]	Expt. [Ref.]
$_2(0,0)^0_1$	−0.487 68					
$_2(0,1)^+_2$	−0.126 08	−0.126 01 [11]	−0.126 05		−0.126 04	−0.128 13 [19]
$_3(1,0)^-_2$	−0.119 28	−0.124 24 [11]	−0.124 40		−0.124 328	
$_3(1,1)^+_3$	−0.057 02	−0.061 65 [14]	−0.062 72	−0.062 72	−0.062 71	−0.062 58 [20]
$_4(2,0)^-_3$	−0.051 63	−0.058 34 [13]	−0.058 57	−0.058 57	−0.058 57	
$_4(2,1)^+_4$	−0.032 82	−0.036 78 [11]	−0.037 15	−0.037 18	−0.037 13	−0.037 14 [20]
$_5(3,0)^-_4$	−0.027 98	−0.034 23 [13]		−0.034 29	−0.034 29	
$_5(3,1)^+_5$	−0.020 67	−0.024 52 [11]		−0.024 52		−0.024 52 [20]
$_6(4,0)^-_5$	−0.016 52	−0.022 58 [10]		−0.022 63		
$_6(4,1)^+_6$	−0.011 74	−0.017 52 [11]		−0.017 36		−0.017 33 [20]

tegrating over Ω, we get

$$\sum_{N'}-\frac{1}{2}\left[\frac{d^2}{dR^2}G_N(R)\delta_{NN'}+2\frac{dG_{N'}}{dR}\left\langle\psi_N\left|\frac{d}{dR}\right|\psi_{N'}\right\rangle+\left\langle\psi_N\left|\frac{d^2}{dR^2}\right|\psi_{N'}\right\rangle G_{N'}(R)\right]+U_N(R)G_N(R)=EG_N(R)\ . \quad (26)$$

The equation can be written as [7]

$$\left[\left[\frac{d^2}{dR^2}+2E\right]\underline{I}-2\underline{U}(R)+\underline{W}(R)\right]\mathbf{G}(R)=\mathbf{0}\ . \quad (27)$$

where

$$\underline{U}(R)=\left\langle\Psi_N\left|\frac{\Lambda^2}{2R^2}+\frac{C}{R}\right|\psi_N\right\rangle \quad (28)$$

and

$$\underline{W}(R)=2\left\langle\psi_{N'}\left|\frac{d}{dR}\right|\psi_N\right\rangle\frac{d}{dR}+\left\langle\psi_{N'}\left|\frac{d^2}{dR^2}\right|\psi_N\right\rangle\ . \quad (29)$$

The first approximation ignores all the couplings between different channels to get a set of uncoupled differential equations:

$$\left[\frac{d^2}{dR^2}+2E-2U_N(R)\right]G(R)=0\ . \quad (30)$$

Each of the potential wells $U_N(R)$ converges to the double ionization limit as before in the case of ^1S states. For each potential well, we can solve Eq. (30) numerically. We use the fifth-order Runge Kutta method to solve this equation. The eigenvalues are given in Table III for H^- and in Table IV for He for $^1P^o$ whereas Table V provides similar results for $^1P^e$ states. The $^1P^o$ states can be loosely described as the NsNp and $(N-1)sNp$ configuration. Similarly $^1P^e$ states can be loosely described as the $(N-1)pNp$ configuration but more suitably with pair quantum numbers [7] as indicated in the tables.

Plots of the eigenvectors ψ_N are also of interest to display their distribution in α and θ_{12}. Figures 7 and 8 show such plots as a function of α, with θ_{12} held fixed at π, for ^1S and $^1P^o$ states, respectively. Our earlier paper [1] on ^1S had not provided such plots. The values of R chosen for these displays are approximately near the minima of the wells, that is, near where $F(R)$ has most of its amplitude. Note the concentration of the lowest ^1S eigenvectors near $\alpha=\pi/4$. The $^1P^o$ states have, however, a node at this point enforced by symmetry [8]. Figure 9 is a similar study of ^1S eigenvectors but now as a function of θ_{12}, with α held fixed at $\pi/4$. This shows that the lowest eigenvector is maximally concentrated near $\theta_{12}=\pi$.

Now we discuss the effects of d/dR and d^2/dR^2 couplings. The matrix $\underline{W}(R)$, which appears in (27), arises from the R dependence of ψ. Because the two matrices $\underline{U}$ and $\underline{W}$ usually do not commute, they cannot be diagonal-

TABLE IV. Eigenvalues (in a.u.) calculated by Eq. (30) for He $^1P^o$ states, where $\lambda_{max}=121$.

	Eigenvalue			
$_n(K,T)^A_N$	Present	Other [Ref.]	Ref. [16]	Expt. [Ref.]
$_2(0,0)^0_1$	−2.139 87	−2.121 60 [10]		
$_2(0,1)^+_2$	−0.679 64	−0.692 80 [17]	−0.693 13	−0.692 98 [21]
$_3(1,0)^-_2$	−0.587 62	−0.597 07 [17]	−0.597 07	
$_3(1,1)^+_3$	−0.311 72	−0.337 60 [10]	−0.335 63	−0.333 92 [22]
$_4(2,0)^-_3$	−0.277 34	−0.270 70 [10]	−0.285 95	
$_4(2,1)^+_4$	−0.177 75	−0.195 56 [11]	−0.194 54	−0.194 4 [23]
$_5(3,0)^-_4$	−0.161 40	−0.168 30 [10]	−0.178 82	
$_5(3,1)^+_5$	−0.114 40	−0.127 99 [11]	−0.126 43	−0.126 1 [23]
$_6(4,0)^-_5$	−0.104 77	−0.111 55 [10]	−0.119 17	
$_6(4,1)^+_6$	−0.079 30	−0.089 24 [11]	−0.088 60	−0.088 1 [23]

TABLE V. Eigenvalues (in a.u.) calculated by Eq. (30) for He and H^- $^1P^e$ states, where $\lambda_{max}=120$.

	He			H^-		
$n(K,T)^A_N$	Present	Ref. [16]	Ref. [14]	Present	Ref. [12]	Ref. [16]
$_3(0,1)^-_2$	−0.583 98		−0.056 25	−0.123 69		
$_4(1,1)^-_3$	−0.277 90	−0.278 99		−0.054 97	−0.056 00	
$_5(2,1)^-_4$	−0.164 21	−0.165 52		−0.031 42	−0.033 05	−0.031 32
$_6(3,1)^-_5$	−0.107 76	−0.109 93		−0.019 37		−0.021 82
$_7(4,1)^-_6$	−0.075 67					
$_8(5,1)^-_7$	−0.058 22					
$_9(6,1)^-_8$	−0.040 61					

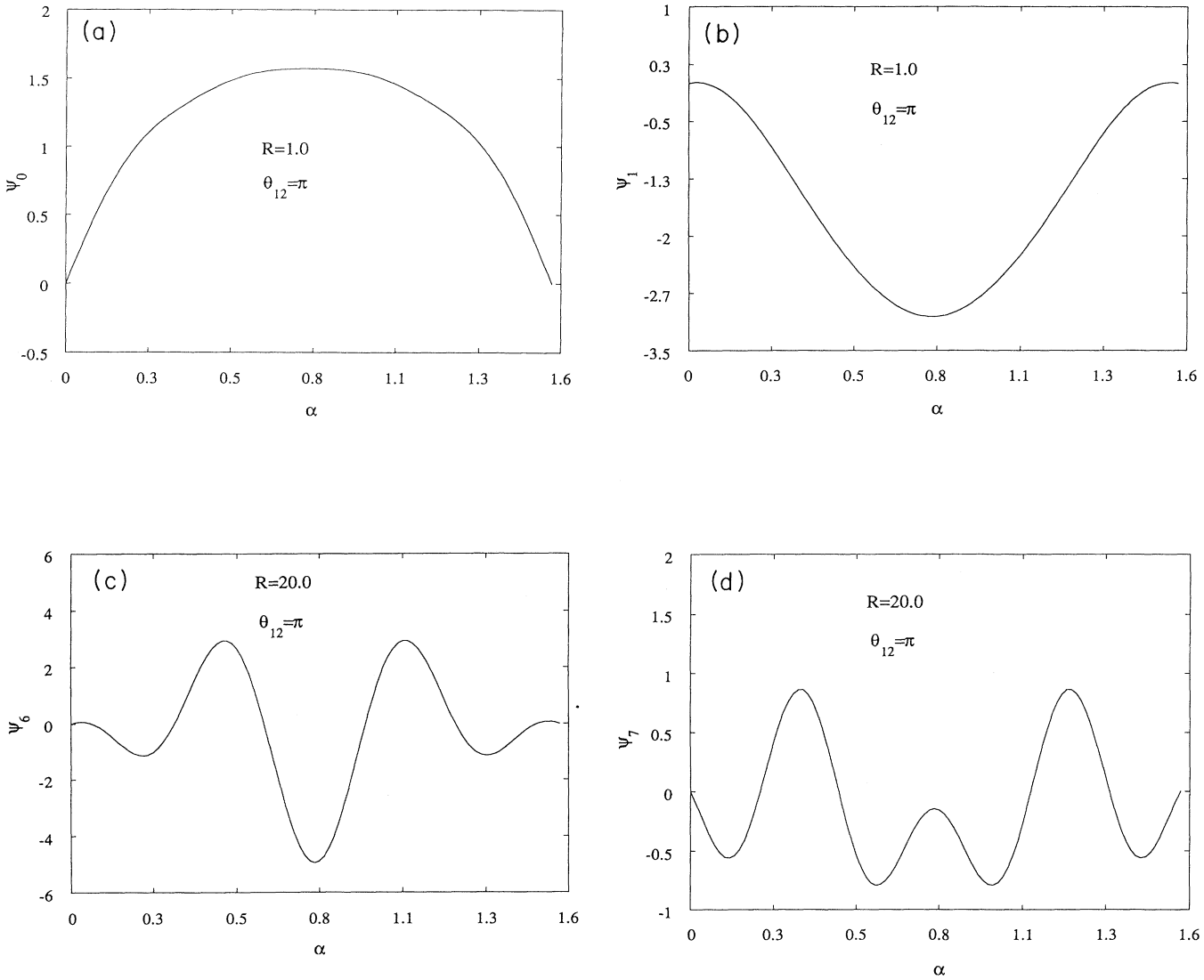

FIG. 7. Eigenvector distributions ψ_N (in arb. units) vs α for ^1S states, $\lambda=12$ and $\theta_{12}=\pi$: (a) the lowest eigenvector, (b) the second lowest eigenvector, (c) the second highest eigenvector, and (d) the highest eigenvector. The value of R (in a.u.) is indicated.

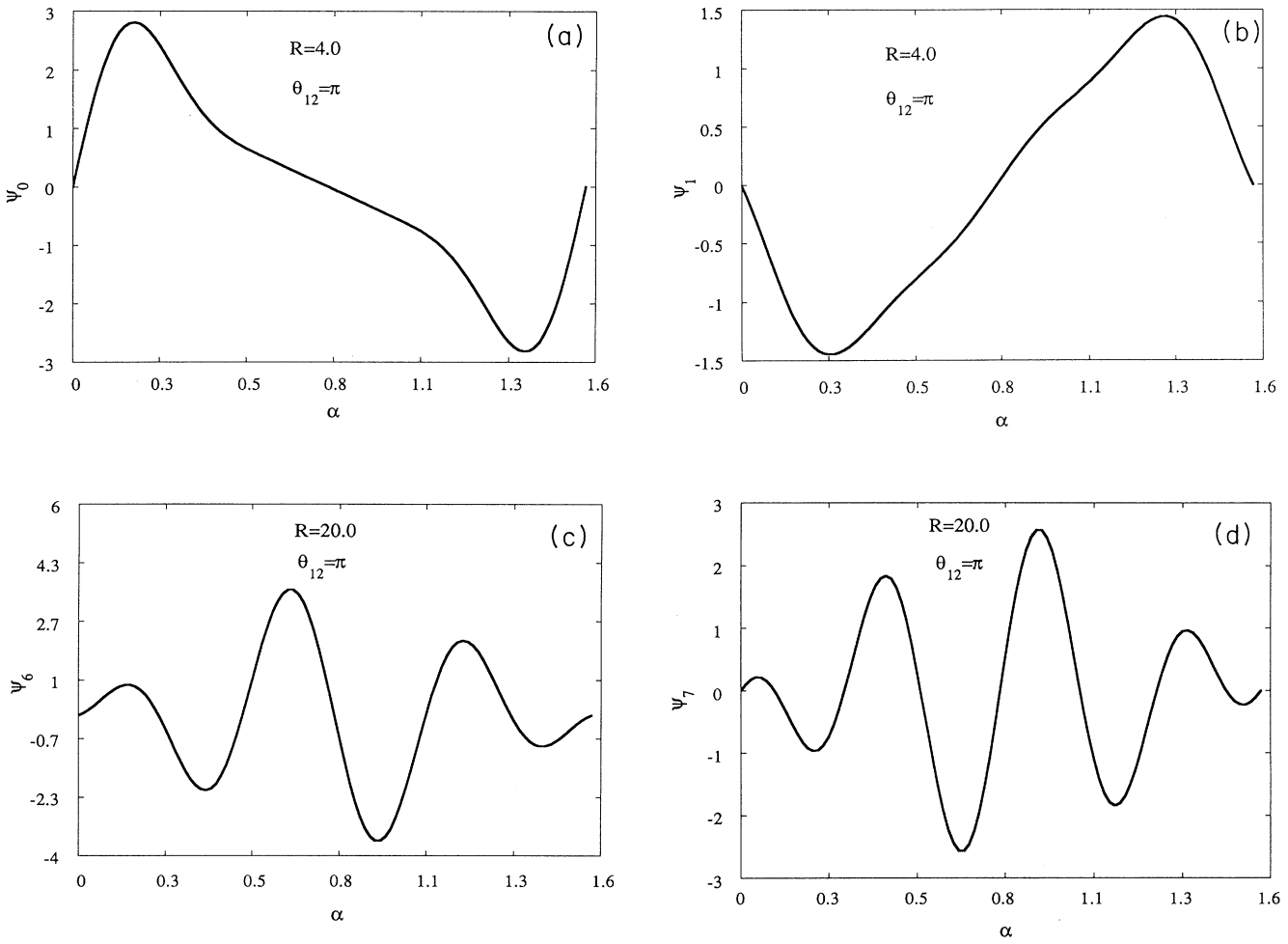

FIG. 8. Eigenvector distributions ψ_N (in arb. units) vs α for $^1P^o$ states, $\lambda=13$ and $\theta_{12}=\pi$: (a) the lowest eigenvector, (b) the second lowest eigenvector, (c) the second highest eigenvector, and (d) the highest eigenvector.

ized simultaneously. But in our case the R dependence comes wholly from the coefficients in $\psi_N=\sum_\lambda a_{N\lambda}(R)\Phi_{\lambda n_{RC}}(\Omega)$. This property makes the problem much simpler, because $\langle\psi_N|\psi_{N'}\rangle=\delta_{NN'}$, and $\langle\psi_N|d\psi_N/dR\rangle=0$, these brackets involving integration over Ω. The $\underline{W}(R)$ term in the Schrödinger equation gives a positive contribution to the energy. Therefore, when we include this term in the Schrödinger equation we will get an upper bound of the energy. In our case $\underline{W}(R)$ can be expressed as

$$\underline{W}(R)=\sum_\lambda a_{N\lambda}(R)\frac{d^2}{dR^2}a_{N'\lambda}(R)+2\sum_\lambda a_{N\lambda}\frac{d}{dR}a_{N'\lambda}\frac{d}{dR}\ . \tag{31}$$

As in the Born-Oppenheimer approximation, if we neglect the off-diagonal term of W, the Schrödinger equation becomes

$$\left\{\frac{d^2}{dR^2}+W(R)+2[E-U(R)]\right\}\mathbf{G}(R)=\mathbf{0}\ . \tag{32}$$

Modifying the Runge-Kutta algorithm, and solving Eq. (32) numerically we get the eigenvalues shown in Table VI for He and H^- in $^1P^o$ states and in Table VII in $^1P^e$ states.

III. RESULTS AND DISCUSSION

Tables I and II give the diagonalization results for the effective charge operator in a λ manifold. Table III gives the eigenvalues for H^-, and Table IV for He in $^1P^o$, and Table V for $^1P^e$, as calculated from (30) with individual potential wells. Tables VI and VII give the improved results from (32) including coupling between wells; these are upper bounds on the energies of the ^1P states. Similarly, by coupling $\lambda=1,3,5,\ldots,121$, $l_1=1$, $l_2=0$, and $S=1$, we get the eigenvalues for $^3P^o$ states, and upon cou-

TABLE VI. Eigenvalues (in a.u.) calculated by Eq. (32) for He and H^- $^1P^o$ states, where $\lambda_{max}=121$ and d/dR and d^2/dR^2 terms are included.

	Eigenvalue	
$_n(K,T)^A_N$	He	H^-
$_2(0,0)^0_1$	−2.115 52	−0.486 20
$_2(0,1)^+_2$	−0.641 31	−0.124 46
$_3(1,0)^-_2$	−0.550 77	−0.117 99
$_3(1,1)^+_3$	−0.284 63	−0.055 92
$_4(2,0)^-_3$	−0.253 45	−0.050 68
$_4(2,1)^+_4$	−0.162 62	−0.031 80
$_5(3,0)^-_4$	−0.147 61	−0.027 10
$_5(3,1)^+_5$	−0.098 43	−0.019 87
$_6(4,0)^-_5$	−0.097 53	−0.015 53
$_6(4,1)^+_6$	−0.074 99	−0.010 82

TABLE VII. Eigenvalues (in a.u.) calculated by Eq. (32) for He and H^- $^1P^e$ states, where $\lambda_{max}=120$ and d/dR and d^2/dR^2 terms are included.

	Eigenvalue	
$_n(K,T)^A_N$	He	H^-
$_3(0,1)^-_2$	−0.579 02	−0.123 31
$_4(1,1)^-_3$	−0.272 59	−0.054 89
$_5(2,1)^-_4$	−0.159 97	−0.030 67
$_6(3,1)^-_5$	−0.104 86	−0.108 73
$_7(4,1)^-_6$	−0.073 92	−0.012 22
$_8(5,1)^-_7$	−0.056 65	
$_9(6,1)^-_8$	−0.039 89	

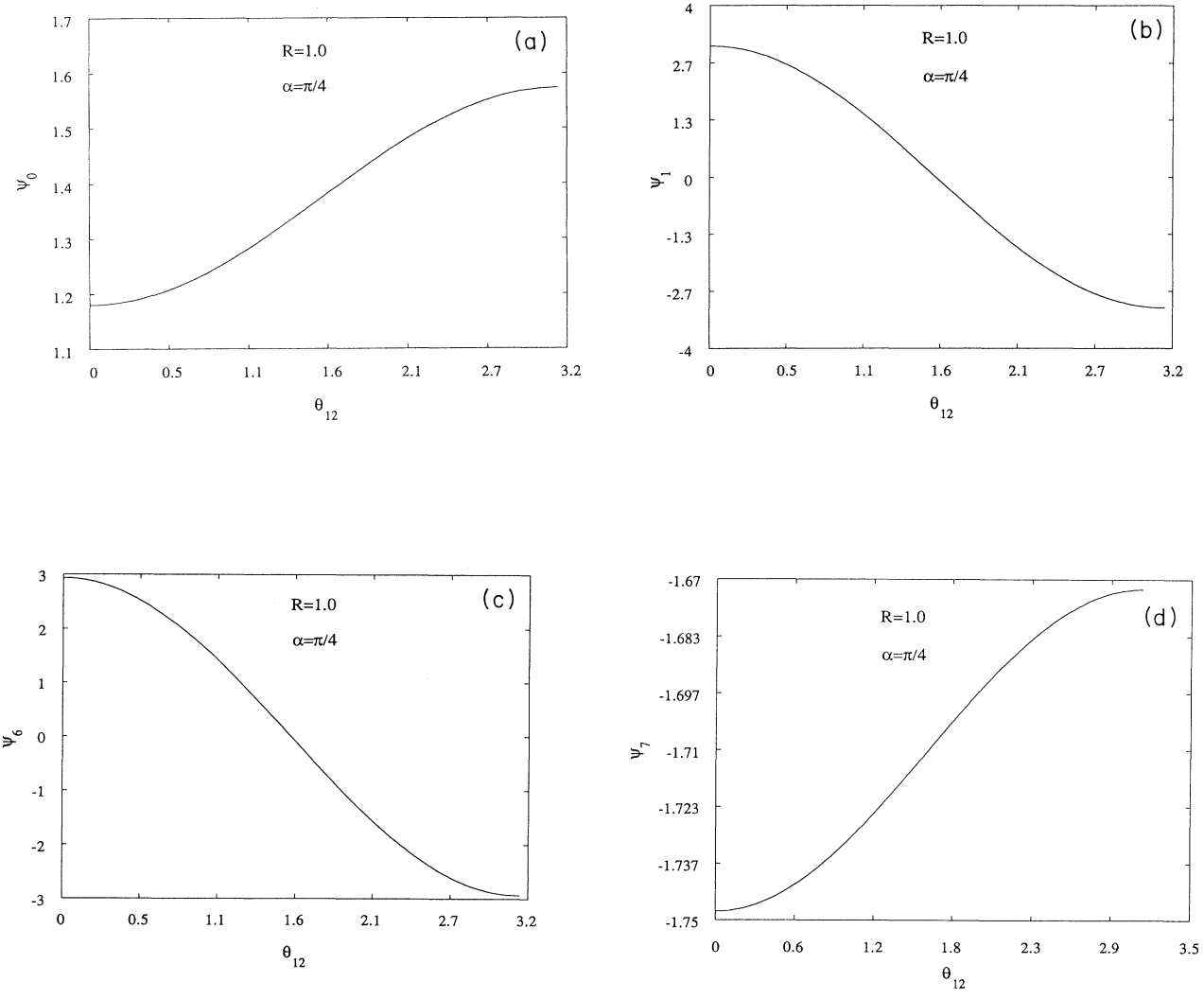

FIG. 9. Eigenvector distributions ψ_N (in arb. units) vs θ_{12} for ^1S states, $\lambda=12$ and $\alpha=\pi/4$: (a) the lowest eigenvector, (b) the second lowest eigenvector, (c) the second highest eigenvector, and (d) the highest eigenvector.

TABLE VIII. Eigenvalues (in a.u.) calculated by Eq. (30) for He and H^- $^3P^o$ states, where $\lambda_{max}=121$.

	He			H^-		
$_n(K,T)^A_N$	Present	Other [Ref.]	Ref. [16]	Present	Other [Ref.]	Ref. [16]
$_2(0,0)^0_1$	−2.156 07			−0.487 87		
$_2(1,0)^+_2$	−0.778 75	−0.781 96 [9]		−0.142 71		
$_3(0,1)^-_2$	−0.573 71	−0.582 81 [9]		−0.119 12	−0.124 25 [14]	
$_3(2,0)^+_3$	−0.360 50	−0.35 [15]	−0.350 38	−0.067 12	−0.068 28 [13]	
$_4(1,1)^-_3$	−0.265 46		−0.279 48	−0.051 47	−0.055 3 [12]	
$_4(3,0)^+_4$	−0.204 73		−0.200 08	−0.038 39	−0.039 59 [12]	−0.039 36
$_5(2,1)^-_4$	−0.152 75		−0.165 14	−0.027 84		
$_5(4,0)^+_5$				−0.024 38	−0.025 68 [18]	−0.025 68

TABLE IX. Eigenvalues (in a.u.) calculated by Eq. (30) for He and H^- $^3P^e$ states, where $\lambda_{max}=120$.

	He			H^-		
$_n(K,T)^A_N$	Present	Ref. [11]	Ref. [16]	Present	Ref. [18]	Ref. [16]
$_2(0,1)^+_2$	−0.709 27	−0.715 19		−0.124 15		
$_3(1,1)^+_3$	−0.340 83		−0.336 09	−0.059 50	−0.063 76	−0.062 76
$_4(2,1)^+_4$	−0.196 28		−0.194 44	−0.034 59	−0.037 23	−0.037 225
$_5(3,1)^+_5$	−0.126 71		−0.126 39	−0.022 42	−0.024 58	−0.024 575
$_6(4,1)^+_6$	−0.087 94			−0.014 68	−0.017 38	
$_7(5,1)^+_7$	−0.063 94			−0.009 85		
$_8(6,1)^+_8$	−0.047 82					
$_9(7,1)^+_9$	−0.034 54					

pling $\lambda=2,6,10,\ldots,118$, $S=1$, $l_1=l_2=1$, and $n_{RC}=(\lambda-2)/2$, we get the eigenvalues for $^3P^e$ states. Table VIII gives the eigenvalues for He and H^- in $^3P^o$ states and Table IX in $^3P^e$. Our P^o results compare favorably with other theoretical calculations in Refs. [9–18] and experimental results in Refs. [19–23]. We also compare our P^e results with Ho's [16] latest results. Our results are accurate to the second digit and may be attributed to our only retaining the dominant potential well in each λ manifold. The main advantage of our method is that it is simple and physically clear. Because we have analytical expressions for most of our matrix elements, our calculations are simple and fast, whereas the other results we compare with need large-scale numerical calculations. We can, therefore, easily extend to very-high-lying doubly excited states, although we do not report the results here because there are no other data to compare with. This method can also be extended to higher L states, with the only added difficulty that analytical expressions for matrix elements are more complicated. Another direction of improvement would be to include more potential wells in each λ manifold to yield more accurate eigenvalues.

ACKNOWLEDGMENTS

We would like to thank Professor Y. K. Ho for providing his newly calculated data before publication. This work has been supported by the National Science Foundation.

*Present address: Department of Physics, California State University, Fullerton, CA 92634.

[1] L. Zhang and A. R. P. Rau, Phys. Rev. A **46**, 6933 (1992).
[2] U. Fano and A. R. P. Rau, *Atomic Collisions and Spectra* (Academic, Orlando, 1986), Chap. 10.
[3] A. R. P. Rau, in *Atomic Physics* **9**, edited by R. S. VanDyck, Jr. and E. N. Fortson (World Scientific, Singapore, 1989), p. 491.
[4] F. H. Read, J. Phys. B **16**, L449 (1977).
[5] I. I. Sobel'man, *Introduction to the Theory of Atomic Spectra* (Oxford, New York, 1972).
[6] L. Zhang, Ph.D dissertation, Louisiana State University, 1992 (unpublished), Chap. 4.
[7] C. D. Lin, Phys. Rev. A **10**, 1986 (1974); Adv. Atm. Mol. Phys. **22**, 77 (1986).
[8] C. H. Greene and A. R. P. Rau, J. Phys. B **16**, 99 (1983).
[9] H. Klar and M. Klar, J. Phys. B **13**, 1075 (1980).
[10] H. Fukuda, N. Koyama, and M. Matsuzawa, J. Phys. B **20**, 2959 (1987); N. Koyama, A. Takofuji, and M. Matsuzawa, *ibid.* **19**, L331 (1986).
[11] H. R. Sadeghpour and C. H. Greene, Phys. Rev. Lett. **65**, 313 (1990); Phys. Rev. A **39**, 115 (1989); H. R. Sadeghpour, *ibid.* **43**, 5821 (1991).
[12] A. Pathak, A. E. Kingston, and K. A. Berrington, J. Phys. B **21**, 2939 (1988); A. Pathak, P. G. Burke, and K. A. Berrington, *ibid.* **22**, 2759 (1989).
[13] R. S. Oberoi, J. Phys. B **5**, 1120 (1972).
[14] D. R. Herrick and O. Sinanoglu, Phys. Rev. A **11**, 97 (1975).
[15] J. Callaway, Phys. Rep. **45**, 91 (1978); Phys. Lett. **68A**, 315 (1978); **81A**, 495 (1981); J. Callaway and J. W. Wooten, *ibid.* **45A**, 85 (1973); J. Callaway, R. S. Oberoi, and G. J.

Seiler, *ibid.* **31A**, 547 (1970); J. Callaway, Phys. Rev. A **26**, 199 (1982); **37**, 3692 (1988); S. Wakid and J. Callaway, Phys. Lett. **78A**, 137 (1980).

[16] Y. K. Ho, J. Phys. B **15**, L691 (1982); Phys. Rev. A **27**, 1887 (1983); **34**, 130 (1986); Z. Phys. D **21**, 191 (1991); Phys. Rev. A **45**, 148 (1992); **48**, 3598 (1993).

[17] D. H. Oza, Phys. Rev. A **33**, 824 (1986).

[18] Y. K. Ho and J. Callaway, Phys. Rev. A **27**, 1887 (1983); J. Phys. B **18**, 3481 (1985); Y. K. Ho, Phys. Rev. A **19**, 2437 (1979); **23**, 2137 (1981); **41**, 1492 (1990), J. Phys. B **23**, L71 (1990).

[19] C. D. Warner, G. C. King, P. Hammond, and J. Slevin, J. Phys. B **19**, 3297 (1986); C. D. Warner, P. M. Rutter, and G. C. King, *ibid.* **23**, 93 (1990).

[20] S. Cohen, H. C. Bryant, C. J. Harvey, J. E. Stewart, K. B. Butterfield, D. A. Clark, J. B. Donahue, D. W. MacArthur, G. Comtet, and W. W. Smith, Phys. Rev. A **36**, 4728 (1987).

[21] R. P. Madden and K. Codling, Astrophys. J. **141**, 364 (1965).

[22] P. Dhez and D. L. Ederer, J. Phys. B **6**, L59 (1973).

[23] M. Zubek, G. C. King, and P. M. Rutter, J. Phys. B **21**, 3585 (1988); M. Zubek, G. C. King, P. M. Rutter, and F. H. Read, in *Proceedings of the 15th International Conference on the Physics of Electronic and Atomic Collisions, Brighton,* edited by J. Geddes, H. B. Gilbody, A. E. Kingston, C. J. Latimer, and H. R. J. Walters (North-Holland, Amsterdam, 1987), p. 1.